GEOPHYSICS, VOL. 66, NO. 2 (MARCH-APRIL 2001); P. 419–427, 8 FIGS., 1 TABLE.

AVO effects of a hydrocarbon source-rock layer

José M. Carcione*

ABSTRACT

The organic content of petroleum source-rock layers can be determined from seismic data with a suitable AVO technique. Since the source rock has a layered structure, the best forward model is a transversely isotropic layer between two isotropic half-spaces, parameterized by the layer thickness and the amount of organic material. This limited number of parameters is essential to obtain a robust inversion method. Here, I compute the *PP*- and *PS*-reflection coefficients of the source bed as a function of layer thickness and organic content, including attenuation mechanisms related to different stages of maturation.

The source rock is modeled as a viscoelastic medium composed of illite/smectite, solid organic matter (kerogen), and fluids (oil and water). The properties of the kerogen/oil/water mixture are obtained with the Kuster and Toksöz model, assuming that oil and water are the inclusion in a kerogen matrix. Then, Backus averaging gives the complex stiffnesses of the layer. To derive the reflection coefficients, I relate the particle velocities and stresses on the top and bottom interfaces between the layer and the substrates.

The results indicate that there is ambiguity regarding the layer thickness, since two or more values can have similar reflection coefficients. For instance, for moderate offsets and 25% kerogen content, the reflection-coefficient curves oscillate with a period of 70 m for *PP*-waves and 40 m for *PS*-waves. On the other hand, the reflection coefficients have a mimimum at approximately 5% kerogen content and increase monotonically above this value. Therefore, the inversion may provide reliable values above approximately 10% kerogen content.

INTRODUCTION

Maps of the regional distributions of organic matter and its maturation level, showing the degree of kerogen-to-oil conversion, are essential for understanding the oil generation and migration processes. Recent petrophysical analyses of petroleum source rocks (Vernik and Landis, 1996) indicate that strong velocity anisotropy can be associated with the presence of organic matter and its distribution in the rock matrix. Hydrocarbon source rocks are laminated structures composed of kerogen, oil, water, and illite layers. When the wavelength of the seismic pulse is much larger than the thickness of the single layers, the finely layered medium behaves as a homogeneous transversely isotropic (TI) material, whose stiffnesses can be obtained by the so-called Backus averaging technique (Carcione, 2000).

A typical situation in the North Sea is represented by the Kimmeridge Shale, a source rock from the Draupne Formation with a maximum thickness of nearly 200 m, overlain by a high-velocity chalk. Detection of the amount of kerogen with AVO methods (Helle and Stovas, 1997) requires a suitable model with a reduced number of parameters. Since the thickness of the source bed is comparable to the seismic wavelength, the model for the AVO analysis must be a layer between two half-spaces. The inversion parameters are the layer thickness and the oil and water saturations. In the case of an immature rock without water, the parameters are the thickness of the layer and the kerogen content. In this framework, I calculate the *PP*- and *PS*-reflection coefficients of a TI layer between two isotropic half-spaces, including dissipation mechanisms attributable to the presence of organic matter and water.

ACOUSTIC PROPERTIES OF THE SOURCE ROCK

I assume the source rock is a layered composite made of illite, kerogen, oil, and water where the amount of oil determines the degree of maturity of the rock. The organic material can be viewed as an amorphous (isotropic) substance subject to liquefaction with increasing temperature and pressure. I assume that the properties of the source rock depend on the maturation stage (Vernik, 1994). From normal pore pressure (immature rock) to high pore pressure (mature rock), the kerogen is gradually transformed to oil. Mature rocks have a more plastic behavior because of their higher hydrocarbon content (HC); therefore, anelasticity is enhanced in this context (Johnston, 1987). The presence of a more compliant and

Manuscript received by the Editor January 11, 1999; revised manuscript received March 24, 2000.
*OGS, Istituto Nazionale di Oceanografia e di Geofisica Sperimentale, Borgo Grotta Gigante 42C, 34010 Sgonico, Trieste, Italy. E-mail: jcarcione@ogs.trieste.it.

liquid-like medium (kerogen + oil and water) triggers new attenuation mechanisms. Moreover, dissipation is also enhanced by the creation of microcracks by hydrocarbon-generation-induced overpressuring.

I consider illite transversely isotropic, the kerogen/oil/water mixture isotropic, and both viscoelastic. Backus averaging gives a TI equivalent medium described by five complex stiffnesses c_{IJ}^* (Schoenberg and Muir, 1989), where

$$\begin{aligned} c_{11}^* &= \langle c_{11} - c_{13}^2 c_{33}^{-1}\rangle + \langle c_{33}^{-1}\rangle^{-1}\langle c_{33}^{-1} c_{13}\rangle^2, \\ c_{33}^* &= \langle c_{33}^{-1}\rangle^{-1}, \\ c_{13}^* &= \langle c_{33}^{-1}\rangle^{-1}\langle c_{33}^{-1} c_{13}\rangle, \\ c_{55}^* &= \langle c_{55}^{-1}\rangle^{-1}, \\ c_{66}^* &= \langle c_{66}\rangle, \end{aligned} \tag{1}$$

with c_{IJ} the complex stiffnesses corresponding to the single constituents. Denoting the proportion of pore material by ϕ (kerogen, oil, and water), the weighted average of a physical quantity a is defined as

$$\langle a\rangle = (1-\phi)a_i + \phi a_p, \tag{2}$$

where the subscripts i and p indicate illite and pore material. The kerogen content is given by

$$K = \phi S_k = \phi(1 - S_o - S_w), \tag{3}$$

where S_k is the kerogen saturation and where S_o and S_w are the oil and water saturations. Note the real porosity, i.e., that related to fluid content, is $\phi(S_o + S_w)$.

For illite, I assume two relaxation functions: M_1 related to dilatational deformations and M_2 related to shear deformations (Carcione et al., 1998). The complex stiffnesses for such TI and viscoelastic medium are

$$c_{I(I)} = \hat{c}_{I(I)} - D + BM_1 + \frac{4}{3}GM_2, \qquad I = 1,2,3, \tag{4}$$

$$c_{IJ} = \hat{c}_{IJ} - D + BM_1 + 2G\left(1 - \frac{1}{3}M_2\right), \qquad I, J = 1,2,3; \quad I \neq J, \tag{5}$$

$$c_{55} = \hat{c}_{55}M_2, \qquad c_{66} = \hat{c}_{66} + G(M_2 - 1), \tag{6}$$

with

$$B = D - \frac{4}{3}G \tag{7}$$

and

$$D = \frac{1}{3}(2\hat{c}_{11} + \hat{c}_{33}), \qquad G = \frac{1}{3}(2\hat{c}_{55} + \hat{c}_{66}), \tag{8}$$

where $\hat{c}_{IJ}$ are the unrelaxed (high-frequency-limit) elastic constants.

Kerogen is described by the complex Lamé parameters given by (Carcione et al., 1998)

$$c_{13} = \rho_k\left(V_{11k}^2 - \frac{4}{3}V_{55k}^2\right)M_1 - \frac{2}{3}\rho_k V_{55k}^2 M_2$$

and

$$c_{55} = \rho_k V_{55k}^2 M_2, \tag{9}$$

where V_{11k} and V_{55k} are the elastic high-frequency-limit compressional and shear velocities and ρ_k is the density. Since the medium is isotropic, $c_{11} = c_{33} = c_{13} + 2c_{55}$ and $c_{66} = c_{55}$.

The following attenuation model assumes a single standard linear solid element (Ben-Menahem and Singh, 1981) describing each anelastic deformation mode (identified by the subscript ν), whose (dimensionless) complex moduli can be expressed as

$$M_\nu(\omega) = \frac{\sqrt{Q_\nu^2+1} - 1 + i\omega Q_\nu \tau_0}{\sqrt{Q_\nu^2+1} + 1 + i\omega Q_\nu \tau_0}, \qquad \nu = 1,2, \tag{10}$$

where ω is the angular frequency. The quality factor associated with each modulus is equal to the real part of M_ν divided by its imaginary part. At $\omega_0 = 1/\tau_0$, the curve quality factor has its highest value Q_ν. For a given angular frequency ω, I take $\tau_0\omega = 1$. The high-frequency limit corresponds to the elastic case with $M_\nu \to 1$.

I consider that the kerogen/oil/water mixture consists of oil/water bubbles embedded in a kerogen matrix. The bulk modulus of the oil/water mixture is calculated by using Wood's equation (Wood, 1941):

$$\frac{S_o + S_w}{K_{ow}} = \frac{S_o}{K_o} + \frac{S_w}{K_w}, \tag{11}$$

where K_o and K_w are the complex moduli of oil and water. The complex stiffnesses of the mixture can be calculated by using the model developed by Kuster and Toksöz (1974). If $s = S_o + S_w$, the stiffnesses are

$$\frac{c_{13}^{(m)} + \frac{2}{3}c_{55}^{(m)}}{K_k} = \frac{1 + [4\mu_k(K_{ow} - K_k)/(3K_{ow} + 4\mu_k)K_k]s}{1 - [3(K_{ow} - K_k)/(3K_{ow} + 4\mu_k)]s} \tag{12}$$

and

$$\frac{c_{55}^{(m)}}{\mu_k} = \frac{(1-s)(9K_k + 8\mu_k)}{9K_k + 8\mu_k + s(6K_k + 12\mu_k)}, \tag{13}$$

where $K_k = c_{13} + 2c_{55}/3$ and $\mu_k = c_{55}$, with c_{13} and c_{55} given in equation (9). The oil and water bulk moduli are given by

$$K_o = \rho_o V_{11o}^2 M_1, \qquad K_w = \rho_w V_{11w}^2 M_1, \tag{14}$$

where V_{11o} and V_{11w} are the elastic high-frequency-limit compressional velocities, M_1 is the dimensionless dilatational modulus, and ρ_o and ρ_w are the densities of oil and water, respectively. The density of the mixture is $\rho_p = S_k\rho_k + S_o\rho_o + S_w\rho_w$, and the rock density is $\rho = (1-\phi)\rho_i + \phi\rho_p$.

REFLECTION COEFFICIENTS OF THE SOURCE-ROCK LAYER

The source-rock layer is located between two lossy isotropic formations, as shown in Figure 1. The anelastic properties of the upper and lower formations are described with the same model used for kerogen [see equations (9) and (10)], where c_{13} and c_{55} play the role of the Lamé constants (see also the appendix). Let us assume that a compressional wave is incident on the plane of vertical symmetry of the orthorhombic source rock. Then, the problem is that of propagation of qP–qS-waves decoupled from the SH-waves. This has been solved by Rokhlin and Wang (1992) for the purely elastic case. However, since the problem

includes dissipation, I reformulate it from the begining using a different approach based on complex slowness components instead of propagation angles as in Rokhlin and Wang (1992). The calculation is developed in the Appendix. For instance, for an incident compressional wave the reflection and transmission coefficient vector $\mathbf{r} = [R_{PP}, R_{PS}, T_{PP}, T_{PS}]^\top$ is given by

$$\mathbf{r} = -(\mathbf{A}_1 - \mathbf{B}\mathbf{A}_2)^{-1}\,\mathbf{i}_P, \tag{15}$$

where $\mathbf{A}_1$ and $\mathbf{A}_2$ are the propagator matrices related to the upper and lower media [equations (A-25) and (A-27), respectively], $\mathbf{B}$ is the propagator matrix of the orthorhombic layer [equation (A-10)], and $\mathbf{i}_P$ is the incidence vector [equation (A-24)].

I assume that the incident wave is a homogeneous viscoelastic wave for which the directions of propagation and attenuation coincide. Then, the horizontal and vertical slowness components are

$$s = \sin\theta / V_{P1}, \qquad s_{P1} = \cos\theta / V_{P1}, \tag{16}$$

where θ is the propagation angle, measured with respect to the z-axis, and V_{P1} is the complex velocity of the upper medium.

EXAMPLES

The material properties of the different media are given in Table 1, where $V_{IJ} = \sqrt{\hat{c}_{IJ}/\rho}$ are the elastic (unrelaxed) velocities (here ρ denotes the density of a single constituent) and where ϵ, γ, and δ denote the unrelaxed anisotropic coefficients introduced by Thomsen (1986). The properties of illite and kerogen are obtained by fitting experimental data for the Kimmeridge Shale provided by Vernik (1995). The clay in this shale is predominantly represented by illite and kaolinite, with the volume percent of smectite varying from 0 to 10% of the rock. The low velocities for illite take into account a fluid softening effect by hydration of the smectite, and the values of the quality factors are based on in-situ measurements for shale at a depth of 1700 m (Hauge, 1981). Additional dissipation mechanisms are englobed in the dilatational quality factor Q_1, assigned to kerogen and oil.

Since illite has a lenticular textural pattern, I assume that only the stiffnesses parallel to bedding are affected. Following Vernik (1994) I modify the stiffnesses c_{11} and c_{66} as

$$c_{11} \to \langle c_{11} \rangle, \qquad c_{66} \to \langle c_{66} \rangle, \tag{17}$$

which incorporate the respective local constants of both illite and kerogen.

The marine Kimmeridge Shale of the Draupne Formation is located between 3480 and 3580 m, and its sonic log is displayed in Figure 2, together with total organic content (TOC)

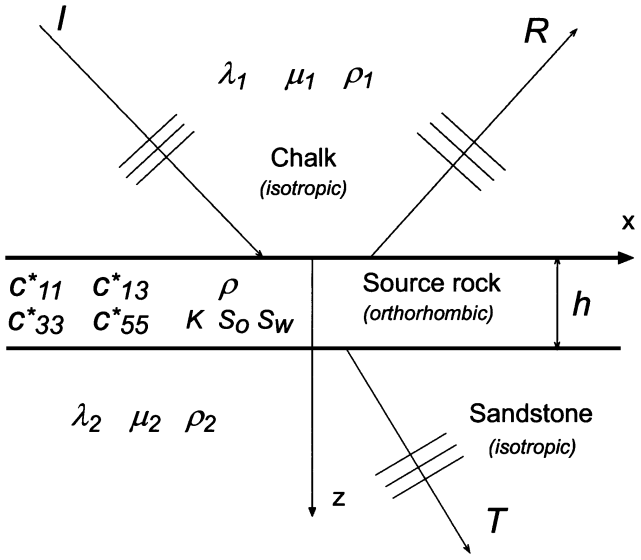

FIG. 1. Diagram showing an orthorhombic layer (source rock) embedded between two isotropic media (chalk and sandstone).

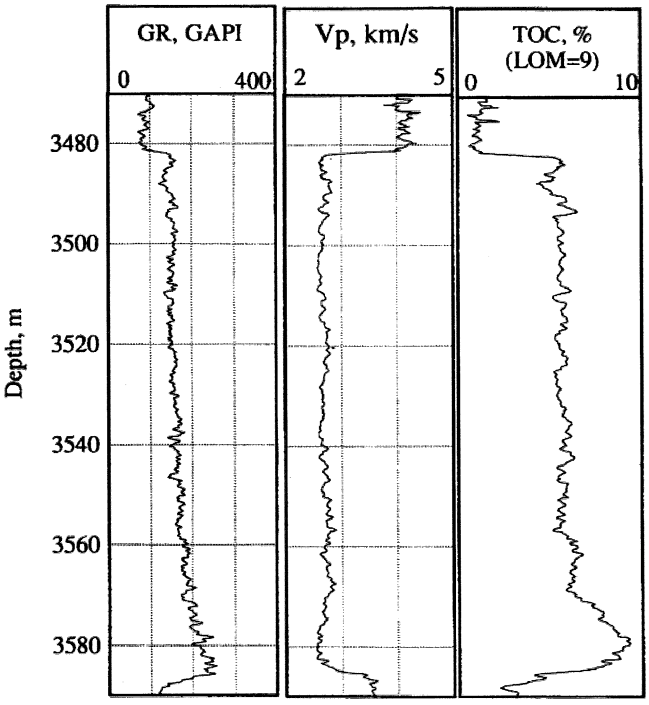

FIG. 2. Log responses of the Kimmeridge Shale, Viking Graben.

Table 1. Material properties.

Medium	V_{11} (km/s)	V_{33} (km/s)	V_{55} (km/s)	V_{66} (km/s)	V_{13} (km/s)	ϵ	γ	δ	ρ (g/cm^3)	Q_1	Q_2
Illite	4.7	4.36	2.46	2.77	2.43	0.08	0.1	−0.05	2.7	270	200
Kerogen	2.6	2.6	1.2	1.2	1.97	0	0	0	1.4	30	20
Oil*	0.73	0.73	0	0	0.73	0	0	0	0.9	10	–
Water	1.5	1.5	0	0	1.5	0	0	0	1.04	10	–
Chalk	4.1	4.1	2.5	2.5	2.08	0	0	0	2.8	200	150
Sandstone	3.6	3.6	1.9	1.9	2.36	0	0	0	2.7	80	50

*Oil/bitumen (McCain, 1984).

values obtained from resistivity measurements (Vernik, 1995). The relation between TOC (in percent) and kerogen content (in percent) is

$$\mathrm{TOC} = \frac{0.75\rho_k \mathrm{K}}{\rho_i - \mathrm{K}(\rho_i - \rho_k)} \tag{18}$$

(Vernik and Nur, 1992). In the area investigated, the source rock is embedded between a chalk and a sandstone with the properties indicated in Table 1. All the examples consider a dominant frequency $f_0 = 25$ Hz.

In the first example, I assume a porosity $\phi = 0.5$, oil saturation $S_o = 0.2$, and water saturation $S_w = 0.2$ (the real porosity is 0.2) and then compute the *PP*- and *PS*-reflection coefficients for different values of the layer thickness h (see Figure 3). For near and medium offsets (from 0° to 30° and 40°) and a given layer thickness, the *PP*-reflection coefficient decreases with increasing incidence angle, whereas the *PS*-reflection coefficient increases. A numerical solution of the reflection problem has been obtained with a 2-D anisotropic and viscoelastic wave-modeling algorithm. This is based on the Fourier method to compute the spatial derivatives and a fourth-order Runge-Kutta technique to compute recursively the wavefield in time (Carcione, 1995). The algorithm uses two standard linear-solid mechanisms to model the dilatational and shear relaxation functions, respectively. The properties of the shale layer are $V_{11} = 2897$ m/s, $V_{33} = 1924$ m/s, $V_{13} = 1245$ m/s, $V_{55} = 914$ m/s, $\rho = 1964$ kg/m^3, $Q_1 = 100$, and $Q_2 = 20$, corresponding to the porosity and saturations indicated above. The numerical mesh has 231×231 points with a grid spacing $D_X = D_Z = 10$ m, and the source is an explosion with a Ricker time history of 25 Hz dominant frequency, located 520 m above the interface. Figure 4 shows a CDP gather of the vertical particle velocity for (a) $h = 0$ m (i.e, no shale layer) and (b) $h = 30$ m. The seismogram in Figure 4a has been enhanced by a factor of six compared with the seismogram in Figure 4b. The first event is the *PP*-reflection, and the second event is the *PS*-reflection. The simulations are in good agreement with the behavior of the curves shown in Figure 3. However, a rigorous approach requires a plane-wave decomposition of the

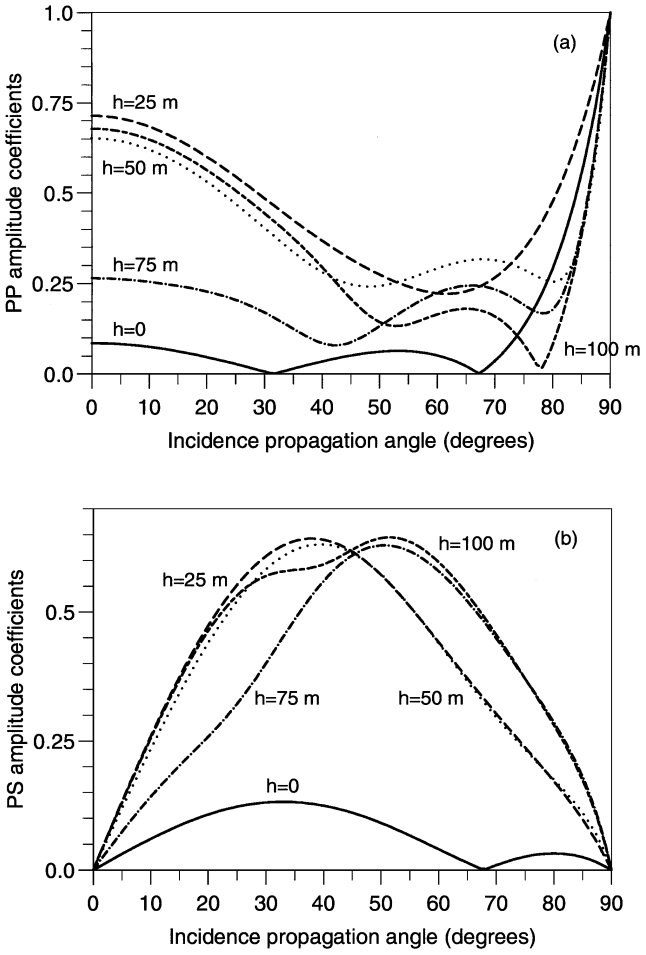

FIG. 3. (a) *PP*- and (b) *PS*-reflection coefficients versus incidence angle for different values of layer thickness h. The kerogen content is $K = 0.3$, and the oil and water saturations are $S_o = S_w = 0.2$.

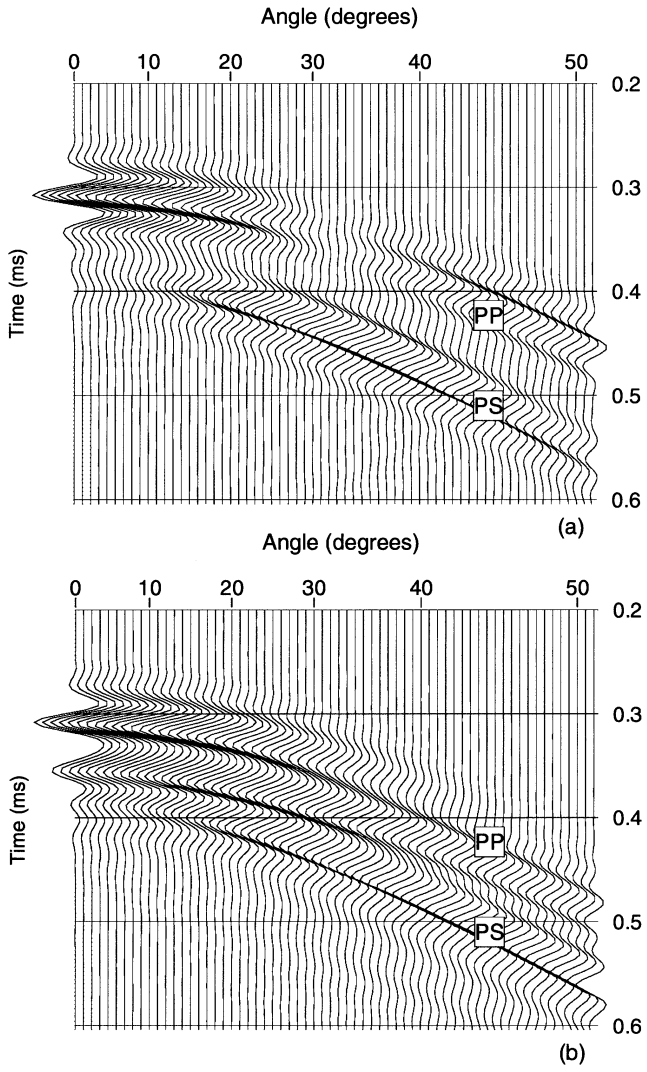

FIG. 4. Common midpoint (CMP) gather of the vertical particle velocity for (a) $h = 0$ m (i.e, no shale layer) and (b) $h = 30$ m. The kerogen content is $K = 0.3$, and the oil and water saturations are $S_o = S_w = 0.2$. The dominant frequency of the source is 25 Hz. The seismogram in (a) has been enhanced by a factor of six compared with the seismogram in (b).

seismograms (for instance, a τ-p transform) and a comparison of the maximum amplitudes to the corresponding reflection coefficients. In addition, one should consider that the reflection coefficients are weighted by the polarization components [see equations (A-14) and (A-15)].

The second example considers $S_o = S_w = 0$, no intrinsic loss, and $\phi = K = 0.2$. The shale consists only of illite and kerogen. Figure 5 represents the *PP*- and *PS*-reflection coefficients for different values of layer thickness h. The curves are qualitatively similar to those of Figure 3. The differences are mainly from the presence of fluids, which modify the stiffness and anelastic properties of the shale.

The following example considers a thickness of $h = 25$ m, $S_o = S_w = 0$, and no intrinsic loss. In this case, I compute the reflection coefficients for different kerogen concentrations (Figure 6). The AVO behavior is similar to the case of varying layer thickness, that is, decreasing *PP*- and increasing *PS*-reflection coefficients for moderate incidence angles.

The *PP*- and *PS*-reflection coefficients versus layer thickness are represented in Figures 7a and 7b, respectively, where the incidence angle is 20°. The oscillatory character of the curves implies an ambiguity of the coefficients with respect to the layer thickness, since two or more values of h may correspond to the same value of the reflection coefficient. The period of the oscillations depends on the frequency and the layer thickness. For instance, the second minimum in Figure 7a is obtained by setting

$$\frac{\omega_0}{V_{ph}} h = \pi,$$

where $\omega_0 = 2\pi f_0$ and V_{ph} is the phase velocity of the *P*-wave in the layer along the the refracted ray. It can be verified that $V_{ph} = 3500$ m/s at 20° incidence angle, implying a minimum value at $h = 70$ m. For increasing (decreasing) frequencies, the period of the oscillations decreases (increases). The same reasoning holds for the shear wave (Figure 7b). In practice, however, this ambiguity can be solved, since for a layer thickness greater than, say, $\pi V_{ph}/(2\omega_0)$, the top and bottom seismic events can in principle be distinguished.

Finally, Figures 8a and 8b show the *PP*- and *PS*-reflection coefficients versus kerogen, where the incidence angle is 20°. There is a minimum value of the reflection coefficients at low kerogen content, approximately at $K_0 = 5\%$. Above this value

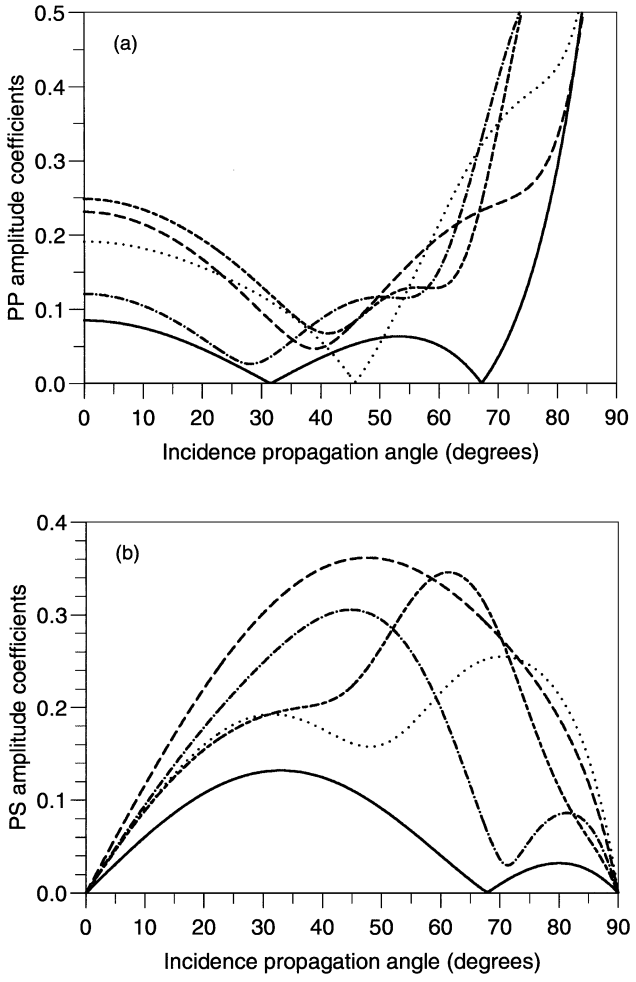

FIG. 5. (a) *PP*- and (b) *PS*-reflection coefficients versus incidence angle for different values of layer thickness h. The kerogen content is $K = 0.2$. There are no fluids ($S_o = S_w = 0$) and no intrinsic loss mechanisms in the shale. The label corresponding to each curve is the same as Figure 1.

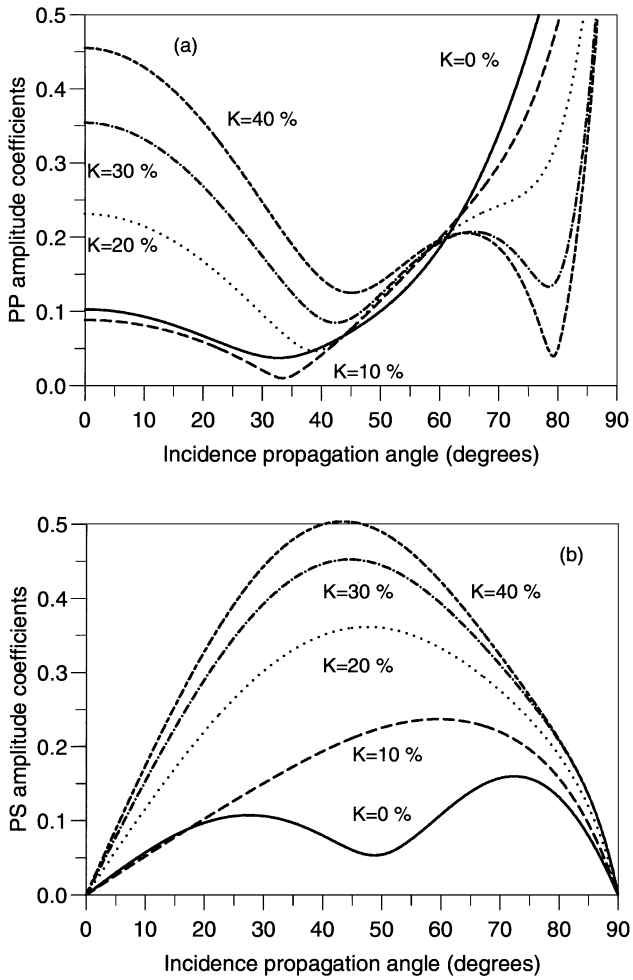

FIG. 6. (a) *PP*- and (b) *PS*-reflection coefficients versus incidence angle for different values of the kerogen content K. Saturation are $S_o = S_w = 0$. The layer thickness h is 25 m.

the coefficients increase monotonically with K. It can be shown that K_0 does not depend on frequency and layer thickness but on the material properties of the source-rock layer. For instance, K_0 increases for increasing V_{11} in the illite layers.

CONCLUSIONS

I investigated the AVO response of a source-rock layer embedded between a chalk and a sandstone, a situation represented by the Kimmeridge Shale in the North Sea. Formally, the problem is to find the *PP*- and *PS*-reflection coefficients of a viscoelastic orthorhombic layer between two viscoelastic isotropic half-spaces. The orthorhombic layer is considered in its plane of symmetry; therefore, it is equivalent to a TI medium.

The use of a limited number of parameters is essential for implementing a robust AVO inversion method. Here, I analyzed the reflection coefficients of the source bed as a function of the layer thickness and organic content. The results of the numerical simulations can be summarized as follows.

1) For near and medium offsets (from 0° to 30° and 40°) and a given layer thickness and kerogen content, the *PP*-reflection coefficient decreases with increasing incidence angle, whereas the *PS*-reflection coefficient increases.
2) For a given kerogen content and incidence angle, the reflection coefficients versus layer thickness have an oscillatory character. The period of the oscillations depends on the frequency of the signal. For instance, for seismic waves of dominant frequency 25 Hz and 20° incidence angle, the period is 70 m.
3) For a given layer thickness and incidence angle, there is a minimum value of the reflection coefficients at low kerogen content—approximately at 5%. Above this value the coefficients increase monotonically with kerogen content. The minimum does not depend on frequency and layer thickness but on the material properties of the source-rock layer.

A straightforward generalization of the method for computing the response of a single layer yields a reflectivity numerical algorithm for computing the response of a stack of anisotropic and viscoelastic layers. The next step of the research is to design a suitable AVO algorithm based on the present forward-modeling tool.

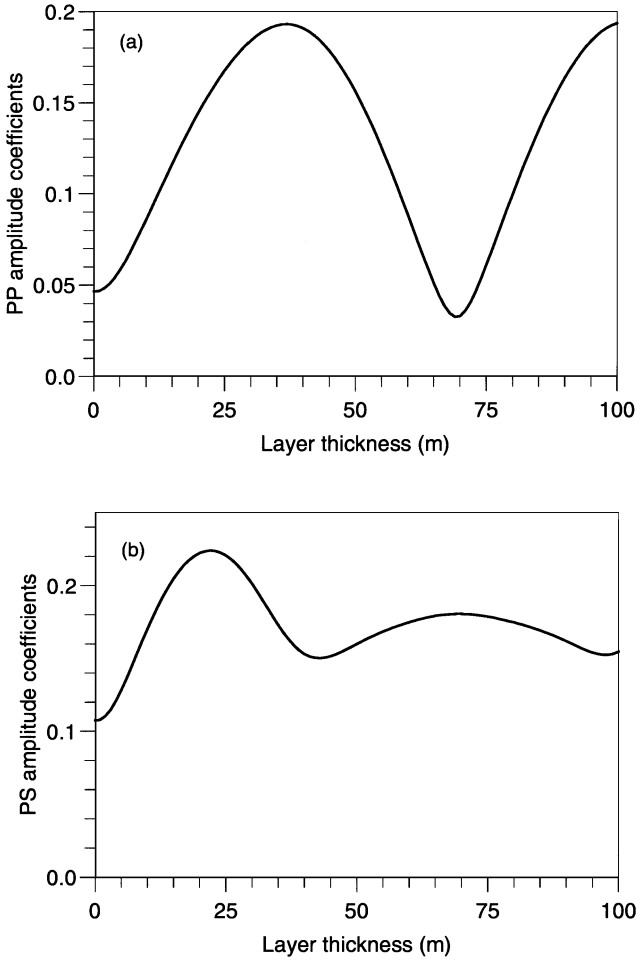

FIG. 7. (a) *PP*- and (b) *PS*-reflection coefficients versus layer thickness h for $\theta = 20°$. The kerogen content K is 0.2. There are no fluids ($S_o = S_w = 0$) and no intrinsic loss mechanisms in the shale.

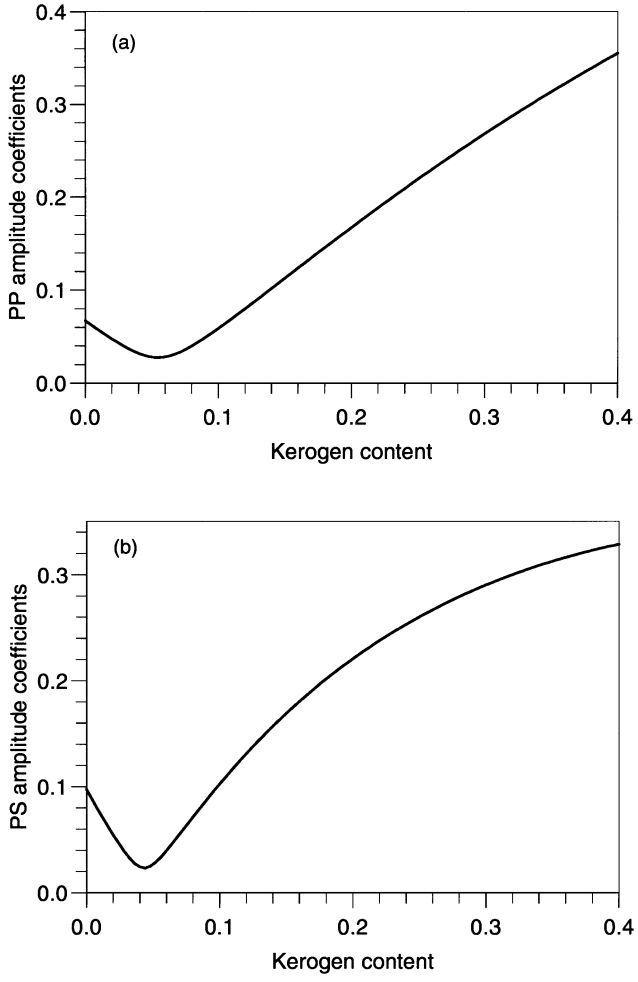

FIG. 8. (a) *PP*- and (b) *PS*-reflection coefficients versus kerogen content K, with $S_o = S_w = 0$. The layer thickness h is 25 m.

ACKNOWLEDGMENTS

This work was supported by Norsk Hydro a.s. (Bergen) with funds of the Source Rock project and by the European Union under the Detection of Overpressure Zones with Seismic and Well Data project. Thanks to Hans Helle for important technical comments.

REFERENCES

Ben-Menahem, A., and Singh, S. G., 1981, Seismic waves and sources: Springer-Verlag Berlin.

Brekhovskikh, L. M., 1960, Waves in layered media: Academic Press Inc.

Carcione, J. M., 1995, Constitutive model and wave equations for linear, viscoelastic, anisotropic media: Geophysics, **60**, 537–548.

——— 1997, Reflection and transmission of qP-qS plane waves at a plane boundary between viscoelastic transversely isotropic media: Geophys. J. Internat., **129**, 669–680.

——— 2000, A model for seismic velocity and attenuation in petroleum source rocks, Geophysics, **65**, 1080–1092.

Carcione, J. M., Cavallini, F., and Helbig, K., 1998, Anisotropic attenuation and material symmetry: Acustica, **84**, 495–502.

Hauge, P. S., 1981, Measurements of attenuation from vertical seismic profiles: Geophysics, **46**, 1548–1558.

Helle, H. B., and Stovas, A., 1997, Source rock properties from seismic data, part I: Marine surface seismic data: E & P Research Centre, Bergen, Norsk Hydro report.

Johnston, D. H., 1987, Physical properties of shale at temperature and pressure: Geophysics, **52**, 1391–1401.

Kuster, G. T., and Toksöz, M. N., 1974, Velocity and attenuation of seismic waves in two-phase media, part I: Theoretical formulations: Geophysics, **39**, 587–606.

McCain, W. D., Jr., 1984, The properties of petroleum fluids: PennWell Books.

Rokhlin, S. I., and Wang, Y. J., 1992, Equivalent boundary conditions for thin orthrotropic layer between two solids: Reflection, refraction, and interface waves: J. Acoust. Soc. Am., **91**, 1875–1887.

Schoenberg, M., and Muir, F., 1989, A calculus for finely layered media: Geophysics, **54**, 581–589.

Thomsen, L., 1986, Weak elastic anisotropy: Geophysics, **51**, 1954–1966.

Thomson, W. T., 1950, Transmission of elastic waves through a stratified solid material: J. Appl. Phys., **21**, 89.

Vernik, L., 1994, Hydrocarbon-generation-induced microcracking of source rocks: Geophysics, **59**, 555–563.

——— 1995, Petrophysics of the Kimmeridge Shale, North Sea: Stanford Rock Physics Laboratory.

Vernik, L., and Landis, C., 1996, Elastic anisotropy of source rocks: Implications for hydrocarbon generation and primary migration: AAPG Bull., **80**, 531–544.

Vernik, L., and Nur A., 1992, Ultrasonic velocity and anisotropy of hydrocarbon source rocks: Geophysics, **57**, 727–735.

Wood, A. B., 1941, A texbook of sound: G. Bell & Sons, Ltd.

APPENDIX

REFLECTION AND TRANSMISSION COEFFICIENTS OF AN ORTHORHOMBIC LAYER BETWEEN TWO ISOTROPIC HALF-SPACES

A plane wave with horizontal complex slowness s is incident on the symmetry plane of the orthorhombic layer from above, as shown in Figure 1. Inside the layer the particle velocity field is a superposition of upgoing and downgoing quasi-compressional (P-) and quasi-shear (S-) waves of the form

$$\mathbf{v} = \begin{pmatrix} v_x \\ v_z \end{pmatrix} = i\omega\left[U_P^- \begin{pmatrix} \beta_P \\ -\gamma_P \end{pmatrix} \exp(i\omega s_P z) + U_S^- \begin{pmatrix} \beta_S \\ -\gamma_S \end{pmatrix} \exp(i\omega s_S z) + U_P^+ \begin{pmatrix} \beta_P \\ \gamma_P \end{pmatrix} \exp(-i\omega s_P z) + U_S^+ \begin{pmatrix} \beta_S \\ \gamma_S \end{pmatrix} \exp(-i\omega s_S z)\right] \exp[i\omega(t - sx)], \quad \text{(A-1)}$$

where ω is the frequency, t is the time variable, U^- are upgoing-wave amplitudes, U^+ are downgoing-wave amplitudes,

$$\beta = pv\left[\frac{c_{55}^* s^2 + c_{33}^* s_z^2 - \rho}{c_{11}^* s^2 + c_{33}^* s_z^2 + c_{55}^*(s^2 + s_z^2) - 2\rho}\right]^{1/2}, \quad \text{(A-2)}$$

and

$$\gamma = \pm pv\left[\frac{c_{11}^* s^2 + c_{55}^* s_z^2 - \rho}{c_{11}^* s^2 + c_{33}^* s_z^2 + c_{55}^*(s^2 + s_z^2) - 2\rho}\right]^{1/2}, \quad \text{(A-3)}$$

where $pv(y)^{1/2}$ denotes the principal value of the square root of the complex number y. The signs + and − correspond to the qP- and qS-waves, respectively, and s_z is the vertical complex slowness, equal to s_P for qP-waves and to s_S for qS-waves. Moreover, β and γ are the horizontal and vertical complex polarizations, respectively (see Carcione, 1997). The complex slowness relation (Carcione, 1997) is solved for s_z, given the horizontal slowness s. It yields

$$s_z = \pm\frac{1}{\sqrt{2}}\left(K_1 \mp pv\sqrt{K_1^2 - 4K_2K_3}\right)^{1/2}, \quad \text{(A-4)}$$

where

$$K_1 = \rho\left(\frac{1}{c_{55}^*} + \frac{1}{c_{33}^*}\right) + \frac{1}{c_{55}^*}\left[\frac{c_{13}^*}{c_{33}^*}\left(c_{13}^* + 2c_{55}^*\right) - c_{11}^*\right]s^2,$$

$$K_2 = \frac{1}{c_{33}^*}\left(c_{11}^* s^2 - \rho\right), \qquad K_3 = s^2 - \frac{\rho}{c_{55}^*}.$$

The signs correspond to

(+, −) downward qP-wave,
(+, +) downward qS-wave,
(−, −) upward qP-wave,
(−, +) upward qS-wave

[the first signs are explicitly given in equation (A-1)].

Normal stresses σ and strains are related by

$$i\omega\sigma_{zz} = c_{13}^* v_{x,x} + c_{33}^* v_{z,z}, \quad \text{(A-5)}$$

$$i\omega\sigma_{xz} = c_{55}^*(v_{x,z} + v_{z,x}) \quad \text{(A-6)}$$

(e.g., Carcione, 1997). Using equations (A-1), (A-5), and (A-6), the velocity-stress vector, inside the layer at depth z, can be written as

$$\mathbf{t}(z) = \begin{pmatrix} v_x \\ v_z \\ \sigma_{zz} \\ \sigma_{xz} \end{pmatrix} = \mathbf{T}(z) \begin{pmatrix} U_P^- \\ U_S^- \\ U_P^+ \\ U_S^+ \end{pmatrix}, \quad \text{(A-7)}$$

where

$$\mathbf{T}(z) = i\omega \begin{pmatrix} \beta_P & \beta_S & \beta_P & \beta_S \\ -\gamma_P & -\gamma_S & \gamma_P & \gamma_S \\ -Z_P & -Z_S & -Z_P & -Z_S \\ W_P & W_S & -W_P & -W_S \end{pmatrix} \times \begin{pmatrix} e^{i\omega s_P z} & 0 & 0 & 0 \\ 0 & e^{i\omega s_S z} & 0 & 0 \\ 0 & 0 & e^{-i\omega s_P z} & 0 \\ 0 & 0 & 0 & e^{-i\omega s_S z} \end{pmatrix}, \quad \text{(A-8)}$$

with

$$W = c_{55}^*(\gamma s + \beta s_z) \quad \text{and} \quad Z = \beta c_{13}^* s + \gamma c_{33}^* s_z. \quad \text{(A-9)}$$

As before, the signs corresponding to the propagation directions are explicitly given in equation (A-8).

Then, the fields at $z = 0$ and $z = h$ are related by the following equation:

$$\mathbf{t}(0) = \mathbf{B}\mathbf{t}(h), \qquad \mathbf{B} = \mathbf{T}(0)\mathbf{T}^{-1}(h), \qquad \text{(A-10)}$$

which plays the role of a boundary condition. Note that when $h = 0$, $\mathbf{B}$ is the identity matrix.

Let the subscript 1 denote the upper half-space and the subscript 2 denote the lower half-space. Moreover, the subscripts I, R, and T denote the incident, reflected, and transmitted waves. Using symmetry properties to define the polarization of the reflected waves, the particle velocities for a P-wave incident from above the layer are given by

$$\mathbf{v}_1 = \mathbf{v}_{P_I} + \mathbf{v}_{P_R} + \mathbf{v}_{S_R}, \qquad \text{(A-11)}$$

$$\mathbf{v}_2 = \mathbf{v}_{P_T} + \mathbf{v}_{S_T}, \qquad \text{(A-12)}$$

where

$$\mathbf{v}_{P_I} = i\omega\big(\beta_{P_1}, \gamma_{P_1}\big)^\top \exp\big[i\omega\big(t - sx - s_{P_1} z\big)\big], \qquad \text{(A-13)}$$

$$\mathbf{v}_{P_R} = i\omega R_{PP}\big(\beta_{P_1}, -\gamma_{P_1}\big)^\top \exp\big[i\omega\big(t - sx + s_{P_1} z\big)\big], \qquad \text{(A-14)}$$

$$\mathbf{v}_{S_R} = i\omega R_{PS}\big(\beta_{S_1}, -\gamma_{S_1}\big)^\top \exp\big[i\omega\big(t - sx + s_{S_1} z\big)\big], \qquad \text{(A-15)}$$

$$\mathbf{v}_{P_T} = i\omega T_{PP}\big(\beta_{P_2}, \gamma_{P_2}\big)^\top \exp\big[i\omega\big(t - sx - s_{P_2} z\big)\big], \qquad \text{(A-16)}$$

$$\mathbf{v}_{S_T} = i\omega T_{PS}\big(\beta_{S_2}, \gamma_{S_2}\big)^\top \exp\big[i\omega\big(t - sx - s_{S_2} z\big)\big], \qquad \text{(A-17)}$$

where

$$\begin{pmatrix} \beta_P \\ \gamma_P \end{pmatrix} = \frac{1}{\sqrt{s^2 + s_P^2}} \begin{pmatrix} s \\ s_P \end{pmatrix}, \quad \begin{pmatrix} \beta_S \\ \gamma_S \end{pmatrix} = \frac{1}{\sqrt{s^2 + s_S^2}} \begin{pmatrix} s_S \\ -s \end{pmatrix}, \qquad \text{(A-18)}$$

with

$$s^2 + s_{P_i}^2 = \frac{\rho_i}{E_i} \equiv \frac{1}{V_{P_i}^2}, \qquad s^2 + s_{S_i}^2 = \frac{\rho_i}{\mu_i} \equiv \frac{1}{V_{S_i}^2}, \quad i = 1, 2, \qquad \text{(A-19)}$$

where V_{P_i} and V_{S_i} are the complex compressional and shear velocities, respectively. On the other hand, the W- and Z-coefficients for the isotropic half-spaces are

$$W_{P_i} = 2\mu_i s_{P_i} s V_{P_i}, \qquad W_{S_i} = \mu_i\big(s_{S_i}^2 - s^2\big)V_{S_i}, \qquad \text{(A-20)}$$

$$Z_{P_i} = \big(\lambda_i s^2 + E_i s_{P_i}^2\big)V_{P_i}, \qquad Z_{S_i} = -2\mu_i s_{S_i} s V_{S_i}, \qquad \text{(A-21)}$$

where $\lambda_i = E_i - 2\mu_i$ and μ_i are complex Lamé constants. Using equations (A-11) and (A-13)–(A-17), the velocity-stress field at $z = 0$ can be expressed as

$$\mathbf{t}(0) = \mathbf{A}_1\mathbf{r} + \mathbf{i}_P, \qquad \text{(A-22)}$$

where

$$\mathbf{r} = [R_{PP}, R_{PS}, T_{PP}, T_{PS}]^\top, \qquad \text{(A-23)}$$

$$\mathbf{i}_P = i\omega\big[\beta_{P_1}, \gamma_{P_1}, -Z_{P_1}, -W_{P_1}\big]^\top, \qquad \text{(A-24)}$$

and

$$\mathbf{A}_1 = i\omega \begin{pmatrix} \beta_{P_1} & \beta_{S_1} & 0 & 0 \\ -\gamma_{P_1} & -\gamma_{S_1} & 0 & 0 \\ -Z_{P_1} & -Z_{S_1} & 0 & 0 \\ W_{P_1} & W_{S_1} & 0 & 0 \end{pmatrix}. \qquad \text{(A-25)}$$

On the other hand, using equations (A-12) and (A-13)–(A-17), the velocity-stress field at $z = h$ can be expressed as

$$\mathbf{t}(h) = \mathbf{A}_2\mathbf{r}, \qquad \text{(A-26)}$$

where

$$\mathbf{A}_2 = i\omega \times \begin{pmatrix} 0 & 0 & \beta_{P_2}\exp\big(-i\omega s_{P_2} h\big) & \beta_{S_2}\exp\big(-i\omega s_{S_2} h\big) \\ 0 & 0 & \gamma_{P_2}\exp\big(-i\omega s_{P_2} h\big) & \gamma_{S_2}\exp\big(-i\omega s_{S_2} h\big) \\ 0 & 0 & -Z_{P_2}\exp\big(-i\omega s_{P_2} h\big) & -Z_{S_2}\exp\big(-i\omega s_{S_2} h\big) \\ 0 & 0 & -W_{P_2}\exp\big(-i\omega s_{P_2} h\big) & -W_{S_2}\exp\big(-i\omega s_{S_2} h\big) \end{pmatrix}. \qquad \text{(A-27)}$$

Combining equations (A-10), (A-22), and (A-26) yields a matrix equation for the reflection and transmission coefficient vector $\mathbf{r}$:

$$(\mathbf{A}_1 - \mathbf{B}\mathbf{A}_2)\mathbf{r} = -\mathbf{i}_P. \qquad \text{(A-28)}$$

The reflection and transmission coefficients R_{SP}, R_{SS}, T_{SP}, and T_{SS} for an incident S-wave have the same scattering matrix as the P incident wave, but the vector $\mathbf{i}_P$ is replaced by

$$\mathbf{i}_S = i\omega\big[\beta_{S_1}, \gamma_{S_1}, -Z_{S_1}, -W_{S_1}\big]^\top. \qquad \text{(A-29)}$$

In the absence of layer h ($h = 0$), $\mathbf{B}$ is the identity matrix, and I get the system of equations obtained by Carcione (1997). When the upper and lower half-spaces are the same medium, the absolute value of the PP-reflection coefficient at normal incidence is given by

$$\frac{2|R_0 \sin(kh)|}{\big|R_0^2 \exp(-ikh) - \exp(ikh)\big|}, \qquad \text{(A-30)}$$

where

$$k = \frac{\omega}{V_P}h, \qquad V_P = \sqrt{\frac{c^*_{33}}{\rho}}$$

and

$$R_0 = \frac{\rho V_P - \rho_1 V_{P1}}{\rho V_P + \rho_1 V_{P1}},$$

with subscript 1 denoting the upper and the lower half-spaces. It is straightforward to generalize this approach for computing the seismic response of a stack of viscoelastic and anisotropic layers. I consider N layers with stiffnesses $c^*_{IJ\alpha}$ and density ρ_α, each of them with thickness h_α, such that the total thickness is

$$h = \sum_{\alpha=1}^{N} h_\alpha. \tag{A-31}$$

Matching boundary conditions at the interfaces between layers, it is easy to show that the matrix system giving the reflection and transmission coefficients is

$$\left[\mathbf{A}_1 - \left(\prod_{\alpha=1}^{N}\mathbf{B}_\alpha\right)\mathbf{A}_2\right]\mathbf{r} = -\mathbf{i}_{P(S)}, \tag{A-32}$$

where $\mathbf{i}_{P(S)}$ is the incidence $P(S)$ vector and

$$\mathbf{B}_\alpha = \mathbf{T}(0)\mathbf{T}^{-1}(h_\alpha), \qquad \alpha = 1, \ldots, N. \tag{A-33}$$

This recursive approach, which is the base of most reflectivity algorithms, dates back to Thomson (1950) and is illustrated by Brekhovskikh (1960, p. 61) for a stack of isotropic and elastic layers.